PAPER

Thickness-dependent band gap of α-In_2Se_3: from electron energy loss spectroscopy to density functional theory calculations

To cite this article: Fengjiao Lyu *et al* 2020 *Nanotechnology* **31** 315711

IOP Publishing Nanotechnology

Nanotechnology **31** (2020) 315711 (10pp) https://doi.org/10.1088/1361-6528/ab8998

Thickness-dependent band gap of α-In_2Se_3: from electron energy loss spectroscopy to density functional theory calculations

Fengjiao Lyu[1], Yuanwei Sun[2], Qin Yang[1], Bin Tang[1,3], Mingqiang Li[2], Zhiwei Li[1], Mei Sun[1], Peng Gao[2], Lin-Hui Ye[1] and Qing Chen[1]

[1] Key Laboratory for the Physics and Chemistry of Nanodevices, Department of Electronics, Peking University, Beijing 100871, People's Republic of China
[2] International Center for Quantum Materials, and Electron Microscopy Laboratory, School of Physics, Peking University, Beijing 100871, People's Republic of China
[3] Academy for Advanced Interdisciplinary Studies, Peking University, Beijing 100871, People's Republic of China

E-mail: yelh@pku.edu.cn and qingchen@pku.edu.cn

Received 14 February 2020, revised 21 March 2020
Accepted for publication 15 April 2020
Published 19 May 2020

Abstract

α-In_2Se_3 has attracted increasing attention in recent years due to its excellent electrical and optical properties. Especially, attention has been paid to its peculiar ferroelectric and piezoelectric properties which most other two-dimensional (2D) materials do not possess. This paper presents the first measurement of the thickness-dependent band gaps of few-layer α-In_2Se_3 by electron energy loss spectroscopy (EELS). The band gap increases with decreasing film thickness which varies from 1.44 eV in a 48 nm thick area to 1.64 eV in an 8 nm thick area of the samples. Further, by combining the improved exchange-correlation potential and proper screening of the internal electric field in an advanced 2D electronic structure technique, we have been able to obtain the structural dependence of the band gap within density functional theory up to hundreds of atoms. This is also the first calculation of a similar type for 2D ferroelectric materials. Both experiment and theory suggest that the variation of the band gap of α-In_2Se_3 fits well with the quantum confinement model for 2D materials.

Supplementary material for this article is available online

Keywords: α-In_2Se_3, thickness-dependent band gap, EELS, DFT, quantum confinement

(Some figures may appear in colour only in the online journal)

1. Introduction

In recent years, atomically thin α-In_2Se_3 has sparked worldwide research interests mainly because it is a model two-dimensional (2D) piezoelectric and ferroelectric [1, 2]. Furthermore, unlike transition metal dichalcogenides (TMDs), bulk α-In_2Se_3 has a direct band gap of about 1.4 eV [3–5], such character is beneficial for light absorption and optoelectric property [6–8]. Due to the quantum confinement effect, 2D semiconductors have been reported to have a remarkable thickness-dependent band gap [9], such as Mo- and W-based TMDs [10], and α-InSe [11], etc. Quereda *et al* have observed that the mechanically exfoliated In_2Se_3 flakes also present a thickness-dependent shift in their optical absorption spectra and the optical band gap has been extracted to change from 1.45 eV for thick flakes to 2.8 eV for 3.1 nm thin flakes [12]. However, the experimental data there does not fit the quantum confinement model well when the thickness is smaller than

20 nm. Surface oxidation has been suggested to explain the discrepancy. To the best of our knowledge, this is the only experimental report on the thickness-dependent band gap of α-In_2Se_3 so far.

Traditionally, the band gap is measured by optical spectroscopies, including absorption, reflection, thermoreflection, transmission, photoluminescence (PL), photoconductivity spectroscopy, etc [4, 5, 10, 12]. However, due to the large spot size and long wavelength of the light source, these methods can only be used to measure the materials with a uniform thickness over a large area. Even when a focused laser is used in micro PL, the spatial resolution is still in the level of micrometers [10]. While, a strong laser may cause irreversible damage to the 2D samples.

Electron energy loss spectroscopy (EELS) in a transmission electron microscope (TEM) or scanning transmission electron microscopy (STEM) allows measurements of optical and electronic properties of a sample with high spatial resolution [13, 14]. With the developments of TEM/STEM (aberration corrector and monocromator) and EELS techniques, low-loss EELS or valence electron energy loss spectroscopy (VEELS) for loss energies lower than about 50 eV carried out through TEM/STEM has been developed to be a powerful method to investigate low-energy excitation in solids with nanoscale spatial resolution, and has been used for measuring the band gap of a variety of materials [13, 15–17]. Even split peaks by excitons have been detected in MoS_2 and other 2D materials [18].

In this work, low-loss EELS in STEM is used to measure the band gap of few-layer α-In_2Se_3 with varied thickness. When the sample thickness decreases from 48 nm to 8 nm ($\approx$8 layers), the band gap is found to increase from 1.44 eV to 1.64 eV, which shows the clear signature of the quantum confinement effect. Assisted by advanced computational techniques in density functional theory (DFT), we have been able to calculate the structural dependence of the band gaps of α-In_2Se_3 covering the range of thickness of our samples. Our calculations strongly imply that the internal electric field within a ferroelectric is effectively screened out, and that the observed quantum confinement effect of the band gap is an intrinsic nature of 2D ferroelectrics, as it is for 2D non-ferroelectrics.

2. Methods

Few-layer α-In_2Se_3 nanosheets were exfoliated from a bulk α-In_2Se_3 sample (bought from HQ graphene) and transferred onto TEM micro grids covered by holey carbon film using a PMMA-assisted method developed by our group [8]. The detail is given in the supporting information. The present α-In_2Se_3 sample has been confirmed to have hexagonal symmetry with a = b = 4.025 Å and c = 19.235 Å, i.e. 2H phase, by our previous x-ray diffraction (XRD), high resolution TEM (HRTEM) and the diffractogram studies [8]. 2H α-In_2Se_3 has a layered structure with each layer containing Se-In-Se-In-Se five atomic layers [19, 20], and its space group has been reported to be $P6_3mc$ (NO.186) [21], as shown schematically in figure 1(a). Figure 1(b) shows a high resolution high-angle annular dark-field (HAADF) STEM image of the α-In_2Se_3 along [0001] direction from the sample area shown in supporting information figure S1 https://stacks.iop.org/Nano/31/315711/mmedia, this image was taken on a FEI Titan TEM equipped with two spherical aberration correctors operated at 300 kV. It can be seen that the Z-contrast [22, 23] in a unit cell (marked by the green dotted lines) is consistent with that shown in figure 1(a) along [0001]. HAADF image is also simulated for 2H α-In_2Se_3 with $P6_3mc$ space group using the parameters for taking the experimental image. The simulated image (the inset in figure 1(b)) fits the experimental HAADF image very well, further confirming that the present α-In_2Se_3 has the 2H structure.

The TEM image of the In_2Se_3 nanosheets used in one of our experiments is taken on a Tecnai F20 TEM and is shown in supporting information figure S2(a). EELS mappings and the corresponding HAADF images showing the area were taken in STEM mode using a Nion U-HERMES200 TEM equipped with both monochromator and aberration corrector. The microscope was operated at 60 kV in order to increase the energy resolution, reduce the damage to the sample, increase the interaction cross-section thus increase the signal to noise ratio (SNR), and reduce the Cherenkov effect in EELS [16, 24]. The sample was tilted away from zone axes to avoid strong diffraction and possible channeling effect when EELS data were recorded. Figures S2(b)–(c) are high magnification HAADF-STEM images of the edge areas pointed by the arrows in figure S2(a). The step-like contrast indicates the thickness changes like steps. EELS mappings are collected from the areas outlined by the boxes in these figures.

3. Results and discussion

First of all, the thickness of the In_2Se_3 nanosheets is characterized through EELS using plasmon peaks, because the samples on holey carbon film are very difficult to measure by atomic force microscopy (AFM), which has been widely used to measure the thickness of thin samples. Figure 2(a) is a HAADF-STEM image showing one sample area. Figure 2(c) is a high magnification HAADF-STEM image of the area outline by the red box in figure 2(a). EELS spectrums containing plasmon peaks are collected in STEM mode in an energy window ranging from -10.07 eV to 92.49 eV using a CCD with 2048 channels from every position where low-loss EELS will be collected. Figure 2(d) is the EELS mapping obtained from the area shown in figure 2(c). Figure 2(b) shows the EELS spectrum from one pixel in figure 2(d), two plasmon peaks can be seen clearly at around 15 eV and 21 eV in the inset enlarged spectrum. The log-ratio method is used to calculate the sample thickness from the EELS spectra. According to Poisson statistics, the thickness (t) of the film can be calculated using the formula:

$$t = \lambda \ln\left(I_{tot}/I_{ZLP}\right)$$

where, I_{tot} is the sum of all counts in the spectrum containing main plasmon signal, I_{ZLP} is the sum of ZLP, λ is the electron mean free path [13]. In this way, the error of the calculated

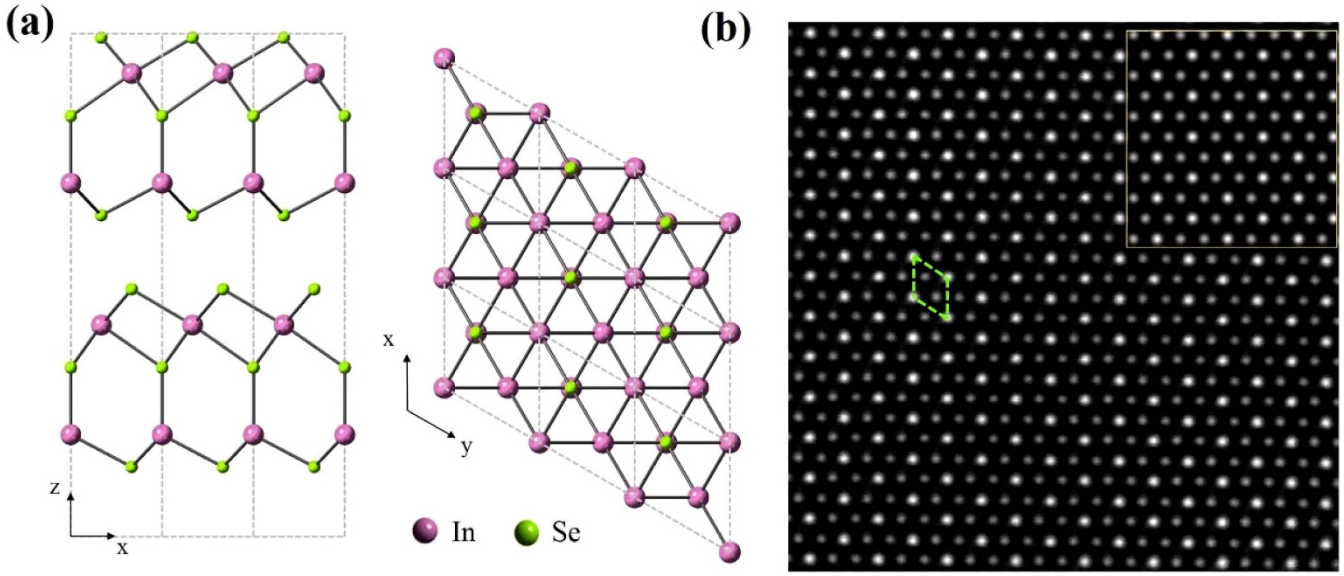

Figure 1. The structure of α-In_2Se_3. (a) The structure model of bulk α-In_2Se_3 projected along the y axis (left) and long z axis (right). The dashed lines indicate the unit cell boundary. (b) STEM image of a few-layer In_2Se_3 nanosheet along the [0001] direction. The green dashed lines outline one unit cell. The inset in (b) is a simulated STEM image calculated using XTEM software.

thickness is less than 10%. The thickness mapping obtained from figure 2(d) is shown in figure 2(e), a step-like thickness change is observed, similar to the HAADF-STEM image in figure 2(c). The areas with the same contrast in figure 2(e) have the same thickness. The three bright dots on the left are due to amorphous carbon deposited when the electron beam is placed there for a long time to align the beam for EELS. Figure 2(f) shows the thickness along the belt marked in figure 2(e), the thickness of the sample increases gradually from the left to the right. The thinnest flat area is 10 nm thick in this sample area.

To measure the band gap of the sample, low-loss EELS STEM mappings are collected using two experimental settings. In the first setting (ST1), the STEM convergence semi-angle is 15 mrad, the EELS collection semi-angle is 24.9 mrad, the energy range is from −0.42 eV to 3.46 eV, and the energy dispersion is 1.9 meV ch^{-1}. In the second setting (ST2), the convergence semi-angle is 20 mrad, the EELS collection semi-angle is 24.9 mrad, the energy range is from −0.699 eV to 5.261 eV, and the energy dispersion is 2.9 meV ch^{-1}. To increase the SNR, we significantly increase the acquisition time (100–200 ms) which only sacrifices the energy resolution slightly.

Figure 3(a) is the low-loss EELS mapping obtained from the area shown in figure 2(c) using ST2. Because collecting a low-loss EELS mapping needs a relatively long time (around 30 min in most of our cases), drift exists, so that the ZLP in the EELS spectra is not always at 0 eV in the original data. Therefore, each spectrum in the image is firstly aligned by ZLP. Figure 3(b) is the EELS mapping generated from figure 3(a) after being aligned by ZLP. The brighter area on the left side in figure 3(b) is in the vacuum. When the sample thickness gradually increases from the left to the right, the brightness in figure 3(b) gradually decreases due to the decreased ZLP. In order to achieve high SNR, we add up the spectra taken from the sample area with the same thickness to obtain one spectrum for one thickness. Figure 3(c) is the spectrum obtained from the area outlined in figure 3(b), the thickness of this area is 10 nm as shown in figure 2. Energy-loss onset can be observed at around 1.5 eV from the enlarged spectrum shown in the inset of figure 3(c). We have checked and confirmed that the carbon contamination does not change the low-loss spectrum. The numbers in the vertical axis in figures 3(c) and (d) are obtained directly from the experimental EELS spectrum. Although these numbers do not equal to the number of electrons being collected, the large value of these numbers does indicate the counting error can be ignored.

The overlap of the extended tail of the ZLP and the energy-loss region is the main error for measuring band gap [25, 26]. The contribution of the ZLP is removed by locally fitting a power-law function in front of the energy-loss onset [16, 27]. To obtain the best fitting, the fitting windows are selected to be about 0.3 eV wide in front of the energy-loss onset. Previously, many people have removed the ZLP using a Fourier-ratio deconvolution with an experimentally recorded vacuum ZLP [13, 17]. However, we cannot do that for the following reasons. In order to obtain as good as possible SNR near the band gap onset, we increased the electron beam density, so that the ZLP in the vacuum area next to the sample in the EELS mapping is saturated. Such saturated ZLP cannot be used to perform deconvolution. Because the electron beam density could be different and the beam may drift from the case of EELS mapping, separately collected ZLP cannot be used to perform deconvolution to the EELS mapping. Also, the sample itself can affect the ZLP, so that the ZLP recorded in the sample area is not the same as that recorded in the vacuum. As the ZLPs in the low-loss spectra recorded from the In_2Se_3 and the vacuum area are very narrow, with the full-width at

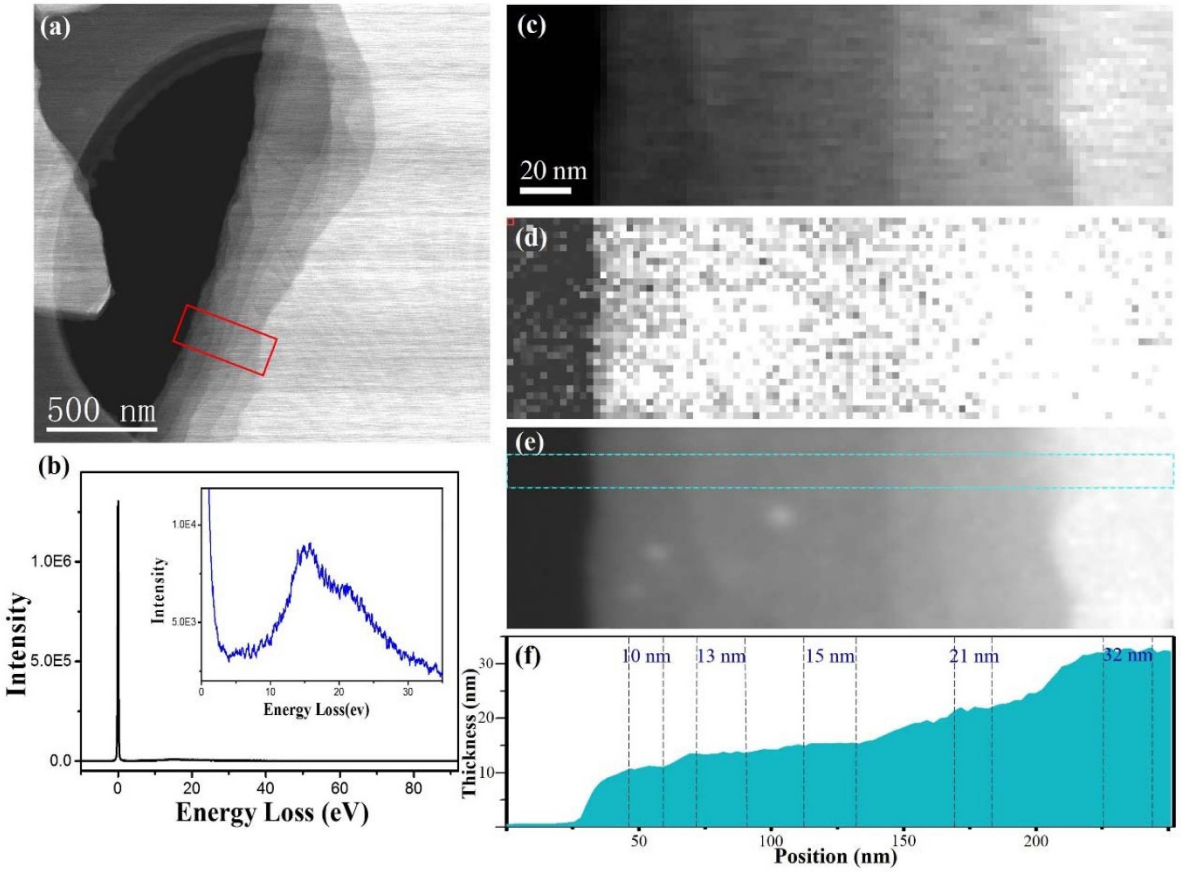

Figure 2. The thickness of few-layer α-In_2Se_3. (a) The HAADF-STEM image of an In_2Se_3 nanosheets obtained by mechanically exfoliation. The red box indicates the area that the EELS mappings are collected. (b) A full-scale raw EELS containing plasmon peaks. The inset diagram shows the enlarged spectrum from 0 eV to 35 eV. (c) The HAADF-STEM image taken from the area outlined by the red box in (a). (d) The EELS mapping image of the In_2Se_3 area outlined in (a) collected in the energy range from −10.07 eV to 92.49 eV. (e) The thickness mapping obtained from (d). (f) The thickness along the belt outlined in (e). Five regions with different thicknesses are selected for further band gap study.

half maximum (FWHM) being smaller than 47 meV in ST1 and smaller than 30 meV in ST2, we accept the energy resolution being the FWHM of the ZLPs and do not perform any deconvolution for the ZLP.

To further increase the SNR, after removing the ZLP, we smooth the spectrum by averaging the original data from ten channels in the case of ST2 (or 15 channels in the case of ST1) along the energy dispersion direction. Since each channel in figure 3(c) is 2.9 meV (1.9 meV in the case of ST1), after smoothing, each channel is 29 meV (28.5 meV in the case of ST1), which is still smaller than the FWHM of the ZLP. The dark line in figure 3(d) is the result obtained by removing the ZLP from that in figure 3(c) and then smoothing by averaging ten channels along the energy dispersion direction, the energy-loss onset can be seen more clearly.

Plural scattering is another factor that complicates the explication of EELS spectrum. Because our samples are very thin (from 8 nm to 48 nm thick), plural scattering should not be a problem. In order to exclude possible impact of plural scattering completely, we perform Fourier-Log (FLOG) deconvolution based on Fourier transform [13, 17] to all the spectra. For the sample thinner than 33 nm, we observe that the spectra are the same before and after FLOG deconvolution, indicating there is no plural scattering in these thin samples.

Before we can claim that the energy-loss onset at around 1.5 eV shown in figure 3(d) corresponds to the band gap of the sample and the thickness-dependent energy-loss onset we will show later does reflect the thickness-dependent band gap, we first consider several effects. The Cherenkov effect, guided light mode and surface losses can hamper the identification of band gap energies by EELS [16, 25, 27, 28]. Cherenkov radiation can be emitted if a charged particle moves faster inside a medium than the light inside this medium [27, 29]. Generally, Cherenkov radiation is linearly dependent on the sample thickness which complicates the study on the thickness-dependent band gap [16, 24]. However, the 60 kV accelerating voltage used in the present work can obviously reduce the Cherenkov effect and guided mode [16, 24]. Importantly, in very thin foils like that in the present work (the sample thickness is significantly smaller than the emitted photon wavelength), the Cherenkov light cone cannot be built up and no Cherenkov radiation can be emitted even if the bulk condition for the emission of Cherenkov radiation is fulfilled [16, 29]. It has been

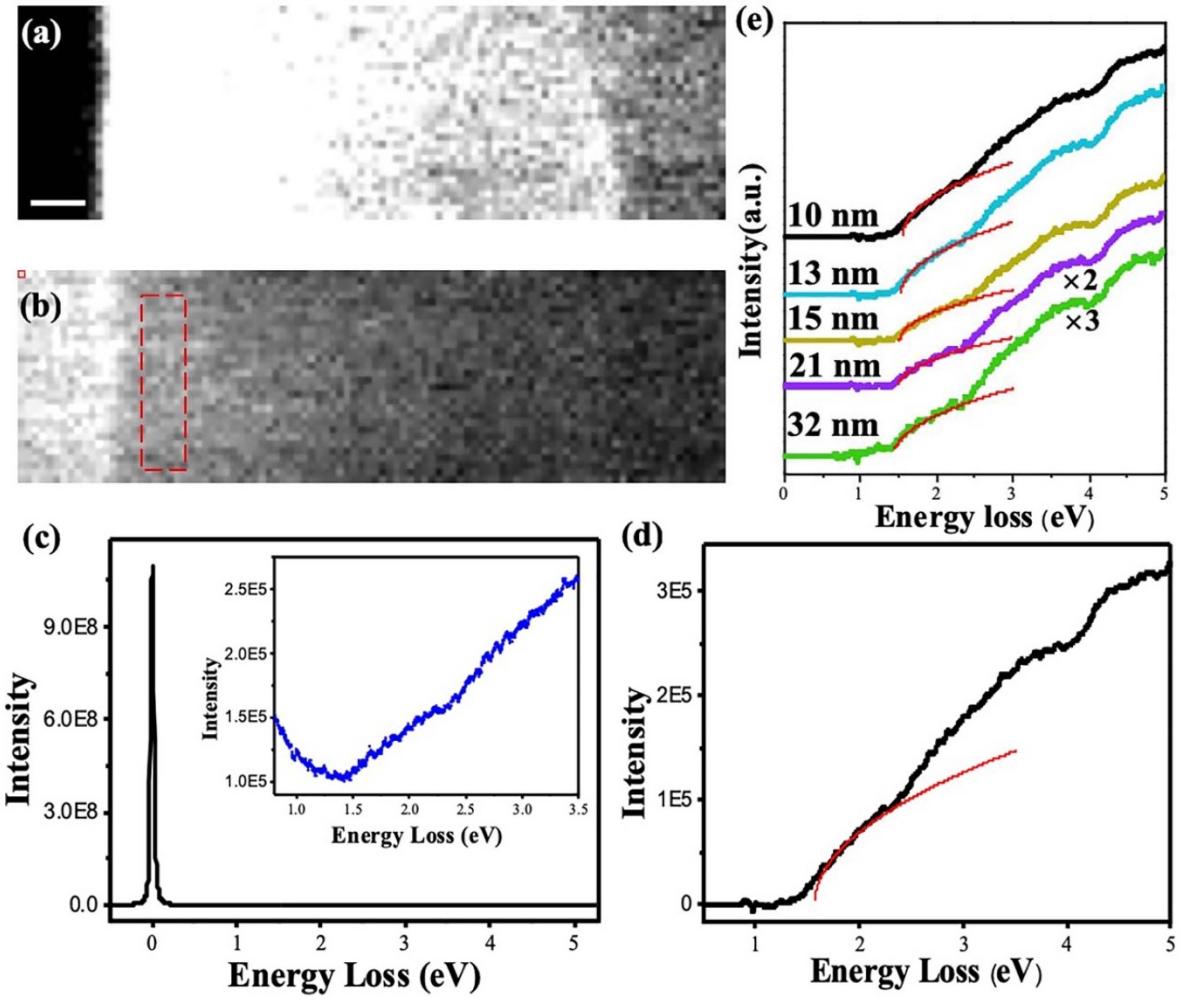

Figure 3. The low-loss EELS of the α-In_2Se_3. (a) The low-loss EELS mapping image of the In_2Se_3 area in figure 2(c) collected in the energy range from −0.699 eV to 5.261 eV. (b) The EELS mapping after calibrating ZLP from (a). (c) A full-scale EELS from the area outlined in (b). The inset image shows the enlarged spectrum from 0.8 eV to 3.5 eV. (d) The dark line is the low-loss EELS obtained after background-subtraction from that in (c) and being smoothed by averaging 10 data points along the energy dispersion direction. The red curve is the fitting curve using a parabolic function. The numbers in the vertical axis in (c) and (d) are obtained directly from the EELS spectrum. (e) The dark line and the coloured lines (except the red lines) are the low-loss EELS spectra from the In_2Se_3 flakes with different thicknesses. The red curves are the fitting curves using parabolic functions.

reported that the probability of Cherenkov losses for TEM foils thinner than 100 nm is very small [16]. For these reasons, the Cherenkov effect can be negligible in the present case.

Guided light modes involve collective excitations of electrons inside the film and can be excited through coupling to Cherenkov radiation. The guided light modes also depend on the thickness of the sample, which can complicate the study on the thickness-dependent band gap [16, 28]. Fortunately, although the guided light mode might appear even below the Cherenkov limit, the shift of the apparent band gap onset affected by the presence of the guided light mode is only several tens of meV between the 5 nm and the 100 nm slices [28]. Such a small shift is about the same as the present experimental error, so that will not affect the present study.

Surface plasmon is a collective excitation mode of the electrons at the surface. It has been suggested that surface plasmons can interfere with the valence loss excitations, thereby making the extraction of the band gap difficult [30]. In the present case, two main plasmon peaks are observed at around 15 eV and 21 eV, as shown in figure 2(b). These two peaks are far away from the energy-loss onset at around 1.5 eV. We observe that as the samples thickness increases, the height ratio of the 15 eV peak to 21 eV peak increases (shown in supporting information figure S3), indicating the peak at 15 eV is a bulk plasmon peak and that at 21 eV is surface plasmon peak.

However, the tail of the plasmon peaks in the low energy end might extend to the energy near the band gap energy and complicate the identification of the band gap onset. To exclude that possibility, we carefully check the so-called *aloof* condition, i.e. the beam in STEM mode is placed right outside the edge of the sample [31]. Although we do observe very small waves in the range from 2.25–4.00 eV, we cannot find any energy-loss signal when the energy is smaller than 2.25 eV in the *aloof* condition EELS (supporting information figure S4), indicating the surface plasmon effect cannot contribute to the energy loss edge at around 1.5 eV as shown

Table 1. The band gap of α-In_2Se_3 with different thickness measured experimentally by low-loss EELS.

Thickness (nm)	8	10	12	13	13	13	15	15	16	19	22	23	28	32	33	48
Band gap (eV)	1.64	1.57	1.54	1.52	1.54	1.52	1.52	1.52	1.51	1.49	1.49	1.48	1.45	1.44	1.45	1.44

The error for most of the data is less than ± 0.03 eV, that for the underlined data is less than ± 0.05 eV.

in figure 3(d). Previous studies have shown that for a thin anisotropic system, such as 2D thin layers, an EELS spectrum is directly related to the parallel (relative to the surface of the 2D layer) dielectric function $\epsilon_{\|}(\omega)$ [32, 33], so that low-loss EELS measures the optical absorption of the system [32, 34]. Therefore, the energy-loss onset at around 1.5 eV in low-loss EELS does correspond to the optical band gap of the sample.

Several methods have been reported to extract band gap energy from low-loss spectra, such as linear fitting [35], parabolic fitting [15, 26, 36], the inflection point approach [26, 37, 38], and direct reading the onset energy in log scale [37], etc. Although the linear fitting method is the most commonly used one for finding the onset energy and band gap [35], the spectrum near the onset around 1.5 eV in the present case is obviously not linear, as shown in figure 3(d). Besides, there are two small bendings at around 2.25 eV and 4.00 eV which could probably be due to surface effect, as energy loss signals can be seen at these energies in the *aloof* condition EELS (supporting information figure S4). Therefore, any fitting we perform to extract the band gap energy should not including the data beyond 2.25 eV in the case shown in figure 3(d).

It has been accepted that the VEELS spectrum reflects the joint density of states, which is described by a parabolic shape at a direct band gap. Through fitting a parabola $(E-E_g)^{1/2}$ to the onset in the spectrum the band gap energy can be extracted at the intersection of the parabola with the energy axis [15, 36]. We observe a parabola can fit the present spectrum very well, as shown in figure 3(d), supporting experimentally that few-layer α-In_2Se_3 has a direct band gap. The intersection of the parabola with the energy axis gives a band gap of 1.57 eV for the sample with 10 nm thickness. By changing the data range for parabolic fitting, we obtain an error of smaller than 0.03 eV for extracting band gap, such error is smaller than the energy resolution of the spectrum.

The low-loss EELS spectra from other areas in this sample with the thickness being 13 nm, 15 nm and 21 nm are also obtained through the same process. Figure 3(e) shows the spectra after background-subtraction and smoothing. To show clearly, the spectra are shifted in the *y* direction. It shows that the spectra near the onset can all be fitted well with parabola. The band gap energies for these thicknesses are then obtained.

A series of EELS are collected from different areas in different samples under the same experimental settings (ST1 or ST2) to avoid other possible effects. Most of the data are like that shown figure 3(d) and can be fitted nicely with parabola. However, in the spectra taken from some sample areas, some energy loss signal can be observed well below 1.5 eV, such as in the spectrum taken from the 32 nm thick area shown in figure 3(e) and that shown in the supporting information figure S5(e). These energy losses have an energy dependence clearly different from a parabolic function. This may be caused by defects and surface contamination [26, 37]. In such cases, as we can still use the parabola to fit the spectra range from 1.5 to 2.25 eV, we can still obtain the band gap energy.

Totally, we obtain the band gap of α-In_2Se_3 for 14 thicknesses in the range from 8 nm to 48 nm. The spectra and fitting lines from an area with the thinnest area being 8 nm thick are shown in supporting information figure S5. All the results we obtained are listed in table 1 and drawn in figure 4. As mentioned previously, the fitting errors are smaller than the experimental energy resolution, the counting error can be ignored, so that the total error is decided by the energy resolution, which is 30 meV for ST2 and 47 meV for ST1. It can be seen from figure 4 and table 1, as the thickness decreases the band gap increases obviously, especially for the samples thinner than 25 nm.

For 2D materials, quantum confinement can influence the band gap [9–12, 39]. The band gap energy E_g of confined 2D nanostructures can be expressed as $E_g^0 = E_{g,bulk}^0 + {}^{A}/_{d^2}$, where $E_{g,bulk}^0$ is the band gap energy of the bulk material, A is the quantum confinement constant, and d is the sample thickness in nm. The present experimentally measured E_g can be best fitted by $E_g^0 = 1.45 + {}^{12.21}/_{d^2}$ (shown in figure 4). The fitting error is ± 0.01 eV, evaluated by using the data with the largest experimental error to do the fitting. This result suggests that the presently observed thickness-dependent band gap is due to quantum confinement effect. Comparing with the previous optical absorption results with an obvious shift between the experimental data and the theoretical curve [12], our experimental results fit the quantum confinement effect very well within the experimental error. The band gap for bulk sample is around 1.45 ± 0.01 eV, which is roughly the same as the band gap of bulk α-In_2Se_3 reported previously. Of course it would be better to measure the thinner sample, or even the monolayer sample. However, as α-In_2Se_3 is a 2D ferroelectric semiconductor, there exist built-in electric fields inside In_2Se_3 [40, 41], the interaction force between the In_2Se_3 layers not only contains the van der Waals force, but also contains the Coulomb interaction. Hence, it is very hard to obtain very thin In_2Se_3 via the mechanical exfoliation method. So far, we have not obtained monolayer In_2Se_3 and we will keep on working for that.

We now turn to the theoretical aspect of our work. First of all, although for non-ferroelectric materials quantum confinement effect of the band gap is widely observed, similar reports for ferroelectrics are relatively rare. In particular, there has been no discussion of this topic for ferroelectrics from first principles calculations. From a naive picture of ferroelectrics, the mere existence of the quantum confinement effect of the band gap seems already extraordinary, because inside the ferroelectrics there should be an internal macroscopic electric field which causes the Coulomb potential to drop within the sample. If the internal field extends over

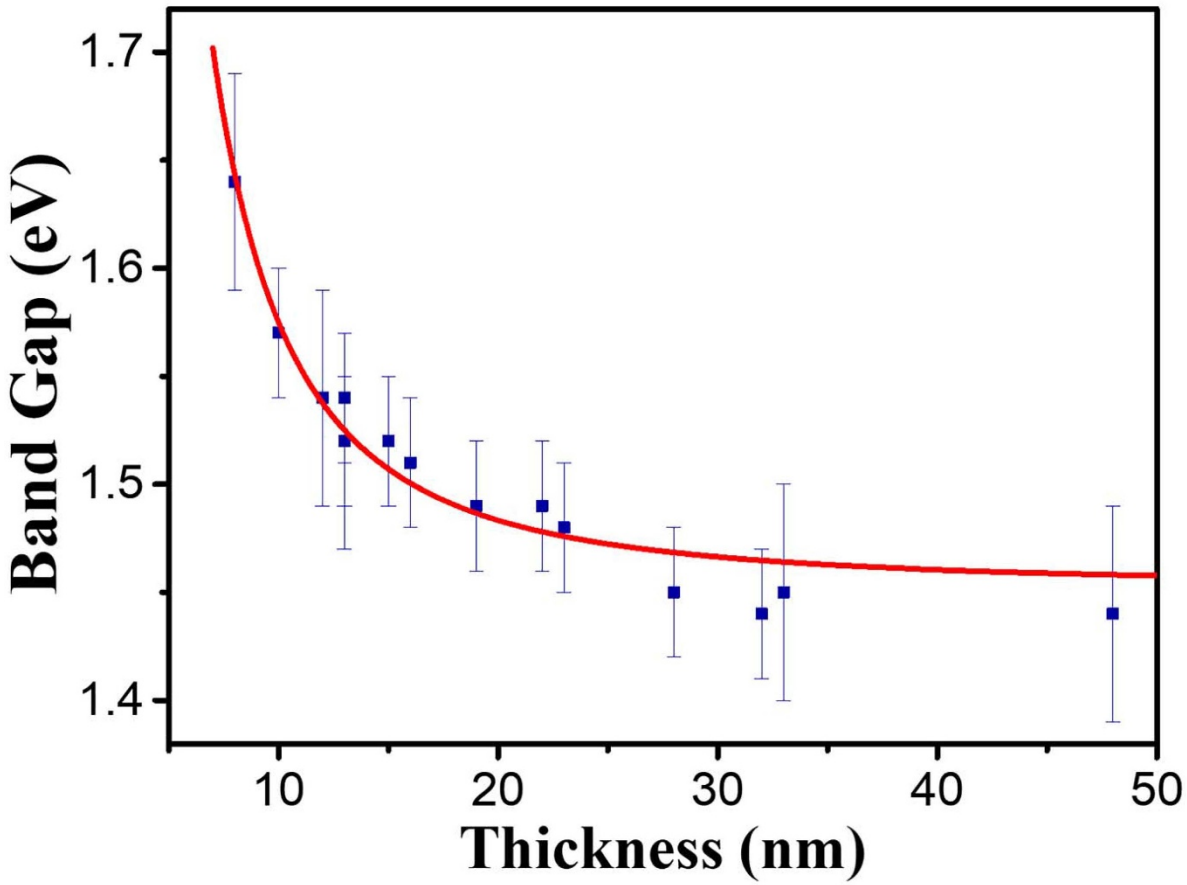

Figure 4. Thickness-dependent band gap of α-In_2Se_3. The dots are the experimental data with error bars. The red curve is the fitting curve using the quantum confinement model.

the whole sample, then the drop of the Coulomb potential increases with the sample thickness, until to a critical thickness electric breakdown happens. Then, the ferroelectrics turns into a metal and the band gap disappears.

The truth that our measured band gap of In_2Se_3 persists up to hundreds of atomic layers implies that the internal electric field does not really extend to long distances. The explanation is that ferroelectric materials are not structurally perfect. Intrinsic defects, adsorbates, surface relaxation, and formation of domains all provide screening mechanism which effectively limit the internal field to small range [42]. In particular, it is known that the typical size of ferroelectric domain is only a few lattice constant [43]. Although within the individual domain the internal field still polarizes the wave functions and brings the conduction bands close to the valence bands, limited by the small size of the domain, the effect is not so strong to completely close up the band gap.

From the methodological point of view, the fundamental gap of the semiconductor can be calculated by the GW approximation (GWA). On top of it, the optical gap can be obtained by adding the excitonic effect from the Bethe–Salpeter equation. This approach, however, is not applicable to the present work since it is computationally too expensive which can barely treat a system of more than 10 atoms. As an alternative, DFT can calculate hundreds of atoms. But this is possible only by using the local exchange-correlation potential. Unfortunately, local potentials usually underestimate band gaps by about 50% because they do not possess the necessary derivative discontinuity at integer electron number [44]. This deficiency may be remedied by using non-local potentials, at the price, however, of quickly increased computational cost.

We shall now summarize all existing calculations of In_2Se_3 which form comparison to our techniques explained later. Let us start from bulk In_2Se_3. Experimentally, the measured optical gap is 1.26 eV–1.45 eV [4, 5, 12, 45, 46], and the exciton binding energy in bulk In_2Se_3 is found to be 0.08 eV. In general, the agreement of theory and experiment is very good.

Film calculation is more difficult. For one quintuple layer of In_2Se_3, local potential of the generalized gradient approximation in the form of Perdew–Burke–Ernzerhof (PBE) [47] gives an indirect band gap of 0.86 eV. Including spin–orbit coupling, the band gap turns to direct and the value is slightly reduced to 0.82 eV. Therefore, the direct and indirect transitions are very close in energy. Further adding GWA correction, the band gap increases to 1.92 eV [46]. One point to note is that, if the direct–indirect band gap transition really happens with an energy difference as small as 0.04 eV, then in experiment this transition cannot be significant.

For films thicker than two quintuple layers, direct calculation by PBE cannot find a band gap and all films are predicted as metal. The error comes from two sources: one is the missing derivative discontinuity in the local potential, and the

other the electric breakdown due to the internal electric field. In the usual computational setup, the In_2Se_3 slabs are formed by stacking multiple quintuple layers together. In this way, the internal field of all quintuple layers point to the same direction, so that the drop of the Coulomb potential across the slab grows linearly with the thickness of the slab. What the PBE calculation found is that at the thickness of two quintuple layers electric breakdown already happens.

In a comparative study [48] of one, two, and three quintuple layers of In_2Se_3 by using the local potential of PBE and non-local potential of HSE06 [49], the electric breakdown is avoided by reversing the atom ordering (and therefore also the dipole moment) of every two quintuple layers. In this way, the internal field is effectively limited within one quintuple layer. The band gaps are found to be 0.88 eV (PBE) and 1.80 eV (HSE06) for one quintuple; and 0.57 eV (PBE) and 1.45 eV (HSE06) for two quintuple layers; and 0.45 eV (PBE) and 1.25 eV (HSE06) for three quintuple layers, respectively. For one quintuple layer, it is noted that the HSE06 band gap is close to the GWA value. The problem with such treatment, however, is that by reversing the atom ordering the structure of the slab is manually altered. Therefore, the calculations correspond to a fictitious material rather than to the real In_2Se_3

With increased film thickness the computational cost of GWA and non-local potential become more and more agonized. In fact, so far there has been no report of a band gap calculation beyond three quintuple layers. For our samples up to about 50 quintuple layers, accurate reproduction of the band gaps fully from first principles is technically impossible. Even so, we emphasize that local potentials can still be used to reveal the quantum confinement effect of the band gap. The reason is that, although the absolute value of the band gap from local potential is not reliable, the chemical trend with structural parameter is often correct. For example, Wei *et al* have successfully calculated the band gap pressure coefficients by use of local potential [50].

Our calculations adapt DFT in the implementation of the full-potential linearized augmented plane wave (FLAPW) method [51]. To account for the exchange-correlation effects, we choose a local potential which is our only choice to calculate hundreds of atoms. Nevertheless, it is still necessary to point out that straightforward use of the simplest local potentials, the local density approximation (LDA) or generalized gradient approximations (GGA), do not suffice our needs, since even for very thin slabs the LDA/GGA band gaps already disappear (see below). To ensure a non-vanishing band gap for the slabs of all thickness, we need a more advanced potential which is local, while capable of restoring (at least partially) the derivative discontinuity. In this work, we choose the Tran-Blaha modified-Becke–Johnson (mBJ) potential [52] for exchange and keep LDA for correlation. mBJ belongs to the family of meta-generalized gradient approximations (meta-GGA). Its computational cost is the same as other local potentials, yet for bulk solids its band gap is as accurate as GWA. For 2D materials the performance of mBJ is not as good as bulk materials, but it is still expected to be better than LDA/GGA.

One obstacle of using mBJ to calculate 2D materials is that it is long-ranged. The problem with long-ranged potentials is that they do not decay to zero at finite distance, and therefore they cannot be correctly represented by supercell. Luckily, the problem of using long-ranged potential for 2D materials has been solved by a recent breakthrough by one of us [53] in which it is suggested that another technique, the authentic slab geometry (ASG) [54], is used to replace the supercell. ASG is specifically developed to calculate 2D materials. It only requires the in-plane periodicity, while perpendicular to the film the potential is allowed to be non-periodic. As is reported [53], ASG works equally well with both short- and long-ranged potentials.

The final issue of using the mBJ potential is a minor one: in the functional form of the mBJ potential there is a c-parameter [52]. For bulk calculation c is calculated by an integral over the unit cell. For film, however, the integral becomes ill-defined. As a simple solution, throughout this work the c-parameter is fixed to 1.28 because this value is found to give consistently good band gaps for 40 bulk semiconductors.

With the exchange-correlation potential being set, we now address the screening of the internal electric field in ferroelectrics. Obviously, a thorough investigation of screening by all possible structural imperfections would be extremely difficult. Here, we simulate the screening effects by a simple approach: we put the In_2Se_3 slab in an external electric field which is tuned to compensate the internal field. In this way, the net macroscopic field within In_2Se_3 becomes zero. Details of the implementation of the external electric field can be found elsewhere [55]. Here we only sketch its main features: The external electric field is generated by two oppositely charged plates with the In_2Se_3 slab being sandwiched in between. During the self-consistency cycles, the total charge on each plate is automatically adjusted so that the external electric field always compensates the internal field within the slab.

With all the above treatments, we have now obtained a computational method which is highly efficient to calculate the band gap of ferroelectric slabs of hundreds of atoms. In this work, this method is used to calculate α-In_2Se_3 slabs from one quintuple layer up to 30 quintuple layers with the maximum film thickness exceeding 57 nm.

To test our method, we first use LDA for exchange-correlation and turn off the compensation field. Only for one quintuple layer we find the band gap to be 0.47 eV. For two quintuple layers and above, all slabs are metallic. Then, we keep LDA for exchange-correlation and turn on the compensation field, the band gaps become 0.79 eV, 0.54 eV, and 0.13 eV for one, two and three quintuple layers, respectively. For four quintuple layers and above all slabs are still metallic.

In the final production calculations, we use mBJ for exchange and turn on the compensation field. As expected, now all slabs are semiconductors. In figure 5 the theoretical band gaps are presented, together with the experimental data and quantum confinement fitting for comparison. Besides, the detailed band structures of three-quintuple layer and eight-quintuple layer films are also presented for comparison in figure S6 of supporting information. At this point, we emphasize that the purpose of our calculations is to reveal the structural dependence of the band gaps rather than to obtain their exact values (which is technically impossible as

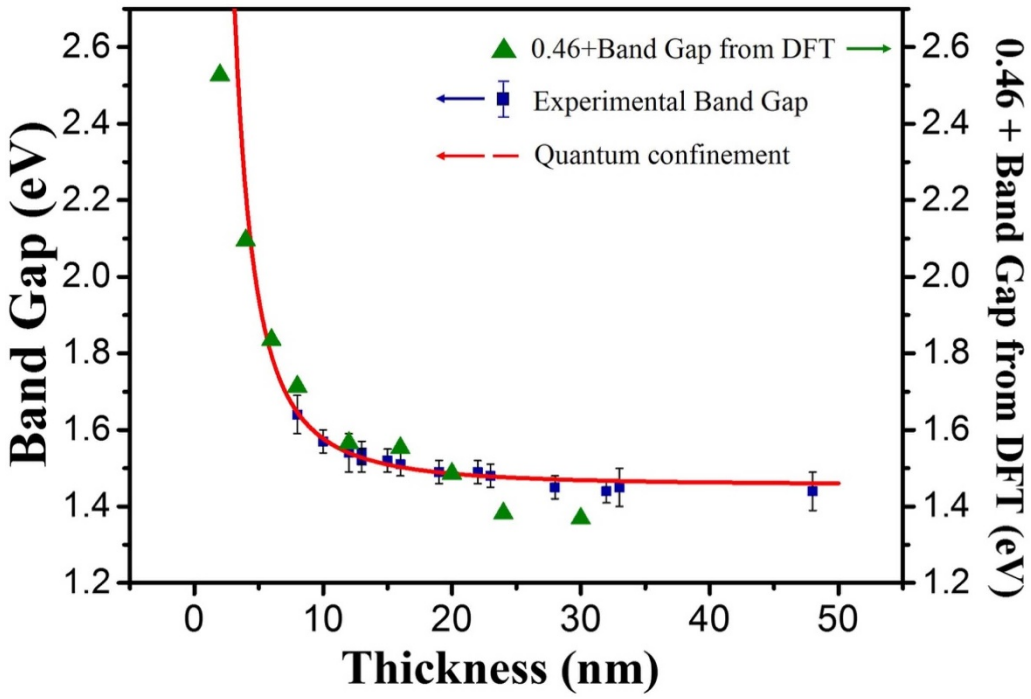

Figure 5. DFT calculation results together with experimental data and fitting curve. The triangle points are the DFT calculated band gap plus 0.46 eV. The square dots with error bars are the experimental data. The red curve is the fitting curve to the experimental data using quantum confinement model.

having been explained in the above). Therefore, in figure 5 all theoretical band gaps are shifted by a constant value of 0.46 eV to form better comparison with the experiment and the fittings. The 0.46 eV shift of the theoretical band gap may be considered a remedy for the remaining deficiency of the mBJ potential as well as the effect of the residue internal electric field. As can be seen from figure 5, the theoretical band gaps also decrease with the increase of the slab thickness which verifies the quantum confinement effect we see from measurements. It shall be noted that in the earlier work [12] the quantum confinement effect of the band gap is also accounted for by the theoretical argument. But that argument is based on the simple infinite potential barrier model instead of from first principles calculation as is present in this work.

4. Conclusions

In summary, we have studied the thickness dependence of the band gap of α-In_2Se_3 nanosheets. Through measuring and fitting the low-loss EELS spectra from exfoliated In_2Se_3 nanosheets, a strong thickness-dependent shift of the optical band gap is observed, ranging from 1.45 eV in a 48 nm to 1.64 eV in an 8 nm thin flakes. Such a thickness-dependent band gap can be well fitted by the quantum confinement effect. To achieve a theoretical understanding of our experimental results, we have calculated the band gap of α-In_2Se_3 up to 30 quintuple layers by DFT, using the mBJ exchange potential to recover the derivative discontinuity and an external, compensation field to avoid electric breakdown. Our calculations show the same trend of band gap variation with the experiment. It suggests that when calculating the electronic structure of 2D ferroelectric materials screening of the internal electric field must be explicitly taken into account.

Acknowledgments

FL, YS and QY made the equal contributions to the article. We thank Professor Lin Gu and Dr. Qinghua Zhang from Institute of Physics, Chinese Academy of Sciences for simulating the STEM image of α-In_2Se_3. This work was supported by the National Key R&D Program of China (Grant No. 2016YFA0200802) and National Natural Science Foundation of China (Grant Nos. 61775006, 1189067, and 61621061). The authors acknowledge Electron Microscopy Laboratory of Peking University for the use of Cs corrected electron microscope.

ORCID iD

Qing Chen https://orcid.org/0000-0002-7919-5159

References

[1] Zhou Y *et al* 2017 *Nano Lett.* **17** 5508
[2] Cui C *et al* 2018 *Nano Lett.* **18** 1253
[3] Julien C, Eddrief M, Kambas K and Balkanski M 1986 *Thin Solid Films* **137** 27
[4] Qasrawi A F 2006 *Thin Solid Films* **514** 267
[5] Ho C H, Lin C H, Wang Y P, Chen Y C, Chen S H and Huang Y S 2013 *ACS Appl. Mater. Inter.* **5** 2269

[6] Island J O, Blanter S I, Buscema M, van der Zant H S J and Castellanos Gomez A 2015 *Nano Lett.* **15** 7853
[7] Jacobs-Gedrim R B, Shanmugam M, Jain N, Durcan C A, Murphy M T, Murray T M, Matyi R J, Moore R L and Yu B 2014 *ACS Nano* **8** 514
[8] Tang B, Hou L, Sun M, Lv F, Liao J, Ji W and Chen Q 2019 *Nanoscale* **11** 12817
[9] Yun W S, Han S W, Hong S C, Kim I G and Lee J D 2012 *Phys. Rev.* B **85** 033305
[10] Mak K F, Lee C, Hone J, Shan J and Heinz T F 2010 *Phys. Rev. Lett.* **105** 136805
[11] Mudd G W *et al* 2013 *Adv. Mater.* **25** 5714
[12] Quereda J, Biele R, Rubio Bollinger G, Agrait N, D'Agosta R and Castellanos Gomez A 2016 *Adv. Opt. Mater.* **4** 1939
[13] Egerton R F 2011 *Electron Energy-loss Spectroscopy in the Electron Microscope* (Berlin:Springer) (https://doi.org/10.1007/978-1-4419-9583-4_1)
[14] Nelayah J, Kociak M, Stephan O, de Abajo F J G, Tence M, Henrard L, Taverna D, Pastoriza-Santos I, Lm L-M and Colliex C 2007 *Nat. Phys.* **3** 348
[15] Rafferty B and Brown L M 1998 *Phys. Rev.* B **58** 10326
[16] Erni R and Browning N D 2008 *Ultramicroscopy* **108** 84
[17] Brockt G and Lakner H 2000 *Micron* **31** 435
[18] Lh G T, Lin Y-C, Mukai M, Sawada H, Lu A-Y, Li L-J, Kimoto K and Suenaga K 2015 *Phys. Rev. Lett.* **114** 107601
[19] Popovic S, Celustka B and Bidjin D 1971 *Phys. Status Solidi* a **6** 301
[20] Han G, Chen Z G, Drennan J and Zou J 2014 *Small* **10** 2747
[21] Kuepers M, Konze P M, Meledin A, Mayer J, Englert U, Wuttig M and Dronskowski R 2018 *Inorg. Chem.* **57** 11775
[22] Pennycook S J and Boatner L A 1988 *Nature* **336** 565
[23] Pennycook S J 1989 *Ultramicroscopy* **30** 58
[24] Canas J, Pinero J C, Lloret F, Gutierrez M, Pham T, Pernot J and Araujo D 2018 *Appl. Surf. Sci.* **461** 93
[25] Stoeger-Pollach M and Schattschneider P 2007 *Ultramicroscopy* **107** 1178
[26] Keller D, Buecheler S, Reinhard P, Pianezzi F, Pohl D, Surrey A, Rellinghaus B, Erni R and Tiwari A N 2014 *Microsc. Microanal.* **20** 1246
[27] Stoeger-Pollach M, Franco H, Schattschneider P, Lazar S, Schaffer B, Grogger W and Zandbergen H W 2006 *Micron* **37** 396
[28] Erni R 2016 *Ultramicroscopy* **160** 80
[29] Gu L, Srot V, Sigle W, Koch C, van Aken P, Scholz F, Thapa S B, Kirchner C, Jetter M and Ruehle M 2007 *Phys. Rev.* B **75** 195214
[30] Stoeger-Pollach M 2008 *Micron* **39** 1092
[31] Huang M R S, Erni R, Lin H-Y, Wang R-C and Liu C-P 2011 *Phys. Rev.* B **84** 155203
[32] Kociak M, Stephan O, Henrar L, Charbois V, Rothschild A, Tenne R and Colliex C 2001 *Phys. Rev. Lett.* **87** 075501
[33] Taverna D, Kociak M, Charbois V and Henrard L 2002 *Phys. Rev.* B **66** 235419
[34] Tizei L H G, Lin Y-C, Lu A-Y, Li L-J and Suenaga K 2006 *Appl. Phys. Lett.* **108** 163107
[35] Park J, Heo S, Chung J-G, Kim H, Lee H, Kim K and Park G-S 2009 *Ultramicroscopy* **109** 1183
[36] Erni R and Browning N D 2005 *Ultramicroscopy* **104** 176
[37] Lazar S, Botton G A, Wu M Y, Tichelaar F D and Zandbergen H W 2003 *Ultramicroscopy* **96** 535
[38] Specht P, Ho J C, Xu X, Armitage R, Weber E R, Erni R and Kisielowski C 2005 *Solid State Commun.* **135** 340
[39] Bastard G, Mendez E E, Chang L L and Esaki L 1982 *Phys. Rev.* B **26** 1974
[40] Yang H, Xiao M, Cui Y, Pan L, Zhao K and Wei Z 2019 *Sci. China Inf. Sci.* **62** 220404
[41] Si M, Saha A K, Gao S, Qiu G, Qin J, Duan Y and Gupta S K 2019 *Nat. Electron.* **2** 580
[42] Landau L D, Bell J, Kearsley M, Pitaevskii L, Lifshitz E and Sykes J 2013 *Electrodynamics of Continuous Media* vol 8 (Amsterdam: Elsevier)
[43] Rabe K, Ahn C H and Triscone J M 2007 *Physics of Ferroelectrics: A Modern Perspective Topics in Applied Physics* (Berlin: Springer)
[44] Perdew J P and Levy M 1983 *Phys. Rev. Lett.* **51** 1884
[45] Ye J P, Soeda S, Nakamura Y and Nittono O 1998 *Jpn. J. Phys. D: Appl. Phys.* **37** 4264
[46] Debbichi L, Eriksson O and Lebegue S J 2015 *Phys. Chem. Lett.* **6** 3098
[47] Perdew J P, Burke K and Ernzerhof M 1996 *Phys. Rev. Lett.* **77** 3865
[48] Hu L and Huang X 2017 *RSC Adv.* **7** 55034
[49] Heyd J, Scuseria G E and Ernzerhof M J 2003 *J. Chem. Phys.* **118** 8207
[50] Wei S H and Zunger A 1990 *Phys. Rev.* B **60** 5404
[51] Wimmer E, Krakauer H, Weinert M and Freeman A J 1981 *Phys. Rev.* B **24** 864
[52] Tran F and Blaha P 2009 *Phys. Rev. Lett.* **102** 226401
[53] Ye L-H 2015 *Phys. Rev.* B **92** 115132
[54] Weinert M, Schneider G, Podloucky R and Redinger J 2009 *J. Phys.: Condens. Matter* **21** 084201
[55] Ye L-H, Luo N, Peng L-M, Weinert M and Freeman A J 2013 *Phys. Rev.* B **87** 075115